A&A 415, 1009–1019 (2004)
DOI: 10.1051/0004-6361:20034160

Astronomy & Astrophysics

BeppoSAX observations of soft X-ray intermediate polars

D. de Martino[1], G. Matt[2], T. Belloni[3], F. Haberl[4], and K. Mukai[5]

[1] INAF–Osservatorio Astronomico di Capodimonte, Via Moiariello 16, 80131 Napoli, Italy
[2] Dipartimento di Fisica, Universita' degli Studi Roma Tre, Via della Vasca Navale 84, 00146 Roma, Italy
e-mail: matt@fis.uniroma3.it
[3] INAF–Osservatorio Astronomico di Brera, Via Bianchi 46, Merate, Italy
e-mail: belloni@merate.mi.astro.it
[4] Max-Planck-Institüt für Extraterrestrische Physik, Giessenbachstraße, Postfach 1312, 85741 Garching, Germany
e-mail: fwh@mpe.mpg.de
[5] Laboratory for High Energy Astrophysics, NASA/GSFC, Code 662, Greenbelt, MD 20771, USA
e-mail: mukai@milkyway.gsfc.nasa.gov

Received 5 August 2003 / Accepted 31 October 2003

Abstract. We present broad-band (0.1–90 keV) spectral and temporal properties of the three Intermediate Polars, RE 0751+144 (PQ Gem), RX J0558.0+5353 (V405 Aur) and RX J1712.6−2414 (V2400 Oph) based on simultaneous soft and hard X-ray observations with the BeppoSAX satellite. The analysis of their spectra over the wide energy range of BeppoSAX instruments allows us to identify the soft and hard X-ray components and to determine simultaneously their temperatures. The black–body temperatures of the irradiated poles of the white dwarf atmosphere are found to be 60–100 eV, much higher than those found in their synchronous analogues, the Polars. The temperature of the optically thin post–shock plasma is well constrained in RX J1712.6−2414 and in RE 0751+144 (13 and 17 keV) and less precisely determined in RX J0558.0+5353. In the first two systems evidence of subsolar abundances is found, similarly to that estimated in other magnetic Cataclysmic Variables. A Compton reflection component is present in RX J0558.0+5353 and in RE 0751+144 and it is favoured in RX J1712.6−2414. Its origin is likely at the irradiated white dwarf surface. Although these systems share common properties (a soft X-ray component and optical polarized radiation), their X-ray power spectra and light curves at different energies suggest accretion geometries that cannot be reconciled with a single and simple configuration.

Key words. accretion, accretion discs – binaries: close – stars: individual: RE 0751+144 (PQ Gem), RX J0558.0+5353 (V405 Aur), RX J1712.6−2414 (V2400 Oph) – X-rays: binaries

1. Introduction

Intermediate Polars (IPs) are the hardest X-ray emitting Cataclysmic Variables (CVs) containing a magnetized white dwarf (WD) that is accreting material from a late-type Main Sequence star. Unlike the strongly magnetized ($B \sim 10$–230 MG) orbitally phase–locked Polars for which $P_{\rm orb} = P_{\rm rot,WD}$, the magnetic field of the white dwarf is not strong enough ($B < 10$ MG) to lock its rotation to the binary orbit and thus $P_{\rm rot,WD} < P_{\rm orb}$. IPs typically populate the long period distribution of magnetic CVs, whilst Polars are generally found at short orbital periods. Hence, the wide orbits and the low magnetic fields in IPs can allow the formation of an accretion disc, which is truncated at the magnetospheric radius. However, other accretion configurations can occurr in IPs, such as the complex disc-overflow, where the stream of matter from the secondary star overpasses the accretion disc and is channeled towards the magnetic poles (Hellier 1991) or the direct (or stream) accretion without an intervening disc. This latter configuration is encountered in Polars, where the accretion material directly flows towards the magnetic poles of the white dwarf.

The X-ray emission in IPs is generally strongly pulsed at the spin $P_{\rm rot} = 1/\omega$ period of the white dwarf, indicating that material accretes onto the magnetic poles via a disc, as it loses memory of the orbital motion (disc-fed systems). This material flows onto the poles in an arc–shaped accretion curtain (Rosen et al. 1988). However, not all systems are found to pulse only at the white dwarf rotation. The presence of additional frequencies in the X-ray power spectra, such as the orbital Ω and the beat (or synodic) $\omega - \Omega$, indicate a disc-overflow accretion whose relative proportion can vary from system to system and with time (Hellier 1991; Wynn & King 1992; Norton et al. 1992). Only one system, RX J1712−24 (V2400 Oph) is known to date to be pulsed at the beat period (Buckley et al. 1997), thus being an unique example of a discless IP.

The X-ray emission of IPs is hard and optically thin ($kT_{\rm Brems.} \sim 5$–30 keV), originating from the post-shock region

Send offprint requests to: D. de Martino,
e-mail: demartino@na.astro.it

above the magnetic pole. These hard X-rays are highly absorbed by cold material (column densities up to $10^{23}\,cm^{-2}$) within the accretion flow (Ishida et al. 1994) and are expected to be reflected by the WD atmosphere (Beardmore et al. 1995; Done et al. 1995; Matt 1999; Ezuka & Ishida 1999; de Martino et al. 2001). Unlike Polars, which also show a strong soft X-ray black-body component (20–50 eV), only three systems, RE 0751+144 (PQ Gem), RX J0558.0+5353 (V405 Aur) and the faint RX J0512.2−3241 (UU Col), were discovered as soft X-ray IPs (Mason et al. 1992; Haberl et al. 1994; Burwitz & Reinsch 2001). The first two are also known to show circular polarized optical emission, suggesting a close link of soft X-ray IPs to the Polars. Indeed the soft X-ray emission in Polars is due to reprocessing, in the white dwarf atmosphere, of hard X-rays and cyclotron radiation, which are emitted from the post-shock region. In particular, the relative proportion of hard-to-soft X-ray emissions was found to depend on the magnetic field strength and local mass accretion rate (Voelk & Beuermann 1998). Hence, the soft IPs might be considered as true non-synchronous Polars and probably as their progenitors. Why most IPs do not show such a soft X-ray component is still an open question.

In this paper we present BeppoSAX observations of RE 0751+144 (PQ Gem) (henceforth RE 0751), RX J0558.0+5353 (V405 Aur) (henceforth RX J0558) and RX J1712.6−2414 (V2400 Oph) (henceforth RX J1712), which together with RX J0028.8+5917 (V709 Cas) (de Martino et al. 2001) are so far the only IPs for which a simultaneous broad-band X-ray coverage has been performed. All three IPs are characterized by circular polarization in their optical emission. Also, while the first two were discovered as soft X-ray IPs by ROSAT, RX J1712 was only recently found by XMM-Newton (Haberl 2002) to possess a soft, but hot (80–100 eV) X-ray component. Here we discuss their temporal and spectral properties over the wide energy range of the BeppoSAX instruments.

2. Observations and data reduction

The BeppoSAX satellite (Boella et al. 1997) performed pointed observations of RX J0558 in Oct. 1996, RE 0751 in Nov. 1996 and RX J1712 in Aug. 1998 with its co-aligned Narrow Field Instruments (NFI), covering the wide 0.1–300 keV energy range, as detailed in Table 1. All three sources were detected with the LECS (0.1–10 keV) and MECS (1–10 keV) instruments.

Due to the failure of one of the three MECS units in May 1997, RX J1712 MECS data were collected by two units. Because of LECS orbital limitations, LECS exposures were much shorter than those of the MECS (but see also Sect. 3.1). The PDS (13–300 keV) is a collimated instrument, which monitors the background continuously switching two (of the four) detectors with a dwell time of 96 s. While RE 0751 and RX J0558 are detected up to 90 keV, for RX J1712, the presence of a bright close-by cluster of galaxies, which heavily contaminates count rates above 13 keV, the PDS data could not be safely extracted.

LECS light curves and spectra have been extracted using a circular region centred on the sources with a radius of 8 arcmin for RE 0751 and RX J1712 and 6 arcmin for the faint RX J0558. The MECS light curves and spectra for all three sources have been extracted with a 4 arcmin radius. While the whole LECS band was used for timing analysis, the spectra from this instrument have been analyzed only below 4 keV due to calibration problems at higher energies. For both intruments, the background was measured and subtracted using the same detector regions during blank field pointings. The PDS light curves and spectra were extracted using a standard routine provided by the BeppoSAX Data Center (SDC). We conservatively extracted the data in the energy range 13–90 keV, above which the sources are hardly detected. The procedure allows rejection of particle background events, as well as spikes caused by single-particle hits, which produce fluorescent cascades that are mainly recorded below 30 keV. The background spectrum is evaluated for each of the two half arrays accumulating the off–source spectra. The background light curves are constructed by linear interpolation between two off–source pointings in each array. Then the spectra and light curves from the two arrays are merged together to construct the background spectrum and light curve for final subtraction.

Net on-source exposure times and count rates for the three sources are reported in Table 1.

3. Timing analysis

A search for periodicities was performed on light curves extracted in the MECS energy range between 1–10 keV. For sake of clarity, the left panels of Figs. 1, 3 and 5 report the extracted light curves with a binning time of 60 s. They show clear periodic pulses on time scale of minutes, with no apparent variability on timescales of hours, implying no orbital modulations.

3.1. The spin pulse characteristics in RX J0558

RX J0558 was discovered as a soft IP by Haberl et al. (1994) with an X-ray period of 272 s. This period is also confirmed by optical photometry (Skillman 1996; Allan et al. 1996). A further detailed re-analysis of the ROSAT data showed that RX J0558 is dominated by the 272 s period below 0.7 keV, whilst at higher energies it shows a 545 s periodicity, indicating that the latter is the spin period of the white dwarf and the soft X-ray period is related to the first harmonic of the spin frequency (Allan et al. 1996). Hence, our timing analysis was done on LECS soft 0.1–0.4 keV, 0.4–1 keV bands and on the whole range of the MECS instrument. The light curves were extracted with a binning size of 68 s (LECS) and 32 s (MECS) and Fourier analysed using the DFT algorithm (Deeming 1975). In order to remove the windowing effects of unevenly sampled data due to the BeppoSAX orbit, the CLEAN algorithm (Roberts et al. 1987) has been applied. The corresponding power spectra (the DFT and CLEANED) are shown in the right panels of Fig. 1. Similarly to the ROSAT observations, they do not reveal the 4.15 h orbital period. A strong peak at 545 s is detected in the MECS band, while below 1 keV no periodicity is found (middle and lower panels).

Table 1. BeppoSAX observations of RX J0558, RE 0751 and RX J1712.

Object	Date	MECS		LECS		PDS		Flux[5]
		T_{expo}(ks)[1]	Count Rates[2]	T_{expo}(ks)[1]	Count Rates[2]	T_{expo}(ks)[3]	Count Rates[4]	
RX J0558	Oct. 7–8, 1996	44.8	0.27	13.7	0.09	84.4	0.32	2.79
RE 0751	Nov. 9–12, 1996	114.7	0.32	27.5	0.15	110.4	0.38	5.30
RX J1712	Aug. 17–19, 1998	82.6	0.50	33.0	0.28	–	–	3.12

[1] Total on-source exposure time.
[2] Net count rates in units of cts s^{-1}.
[3] PDS total exposure times relative to two units (see text).
[4] PDS net count rates in 13–90 keV range.
[5] 0.1–10 keV phase averaged absorbed flux in units of 10^{-11} erg cm^{-2} s^{-1} as derived from best fit parameters in Table 2.

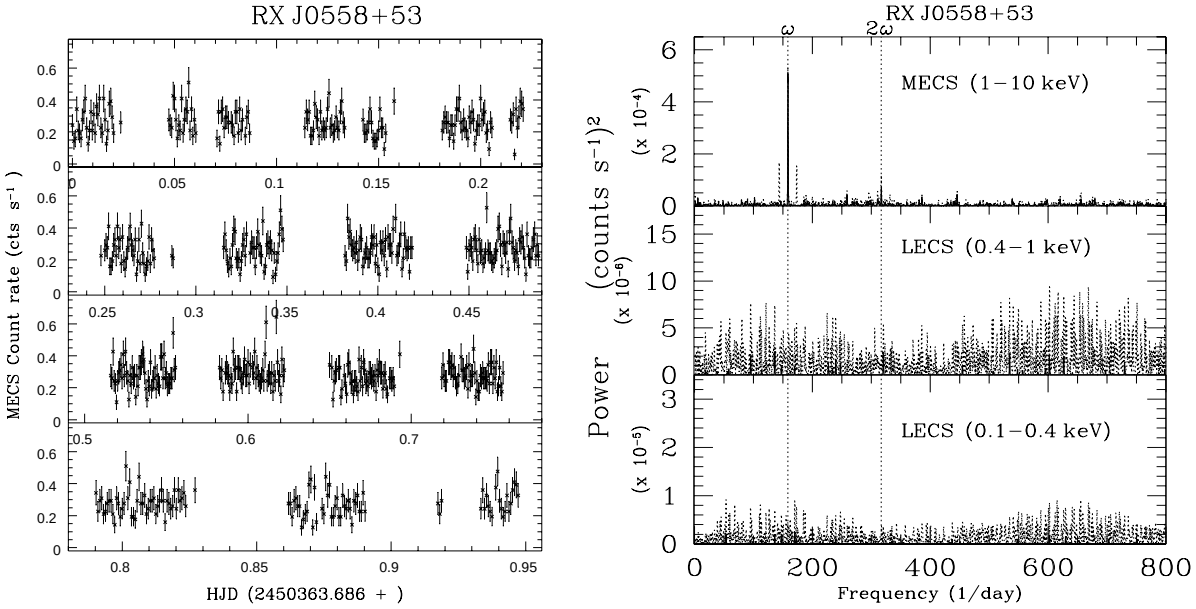

Fig. 1. Left: the net MECS 60 s binned light curve of RX J0558. **Right:** the DFT (dotted line) and CLEANED (solid line) spectra in the MECS (1–10 keV), and two LECS (0.1–0.5 keV) and (0.5–1 keV) bands, show a strong signal at the 545 s rotational period of the white dwarf only in the MECS band.

Differently from the ROSAT data, the first harmonic is also clearly detected in the hard X-rays. Consistency checks on the LECS 1–10 keV band show that the 545 s period is present but at a very low level. As noted in Sect. 2., the effective exposure of LECS instrument was very short (~14 ks) over a 65 ks of observing time, during which no data were acquired for ~16 ks. We then performed separate analysis of the first (19 ks) and second (25 ks) interval, having an effective on-source time of ~7 ks only. We could detect the 545 s modulation only in the first interval, implying that the lack of detection of the soft X-ray modulation is due to the low quality of LECS data and to the small number (~25) of spin cycles covered. Here we note that ASCA observations carried out during the same period and simultaneously with SAX for ~5 hrs confirm the presence of the 272 s modulation in the soft 0.4–0.6 keV band with an amplitude of ~34% (Mukai et al. 1997). Hence the LECS soft X-ray band for this source will not be discussed further for variability purposes.

Allan et al. (1996) provide a spin ephemeris based on the soft X-ray double-humped light curve. The time of their maximum, however, does not correspond to the maximum observed in the hard X-rays and therefore the MECS light curve has been fit with a composite sinusoidal function accounting for the base and second harmonic frequencies. We derive:

$$\mathrm{HJD}_{\max} = 2\,450\,364.159695(2) + 0.006311(6) \times E.$$

This ephemeris is less precise than the one derived from ROSAT data (Allan et al. 1996), probably due to the low statistics of the BeppoSAX light curve and to the non sinusoidal shape of the hard X-ray pulsation. However, it allows a proper phasing of the hard X-ray maximum as shown in Fig. 2, left panel. As for the LECS instrument, the lack of modulation in the high energy PDS data is probably due to the limited quality. As expected, the modulation in the 1–10 keV band is not sinusoidal with a broad shoulder maximum and a shallow minimum and hints of a secondary pulse feature. The pulsed fraction (max-min/average) is 56% in the 1–2 keV band and ~40–45% in the 2–5 keV and 5–10 keV bands. The hardness ratios [2–5/1–2 keV] and [5–10/2–5 keV], tracing the hard component (right panels of Fig. 2 do not show significant

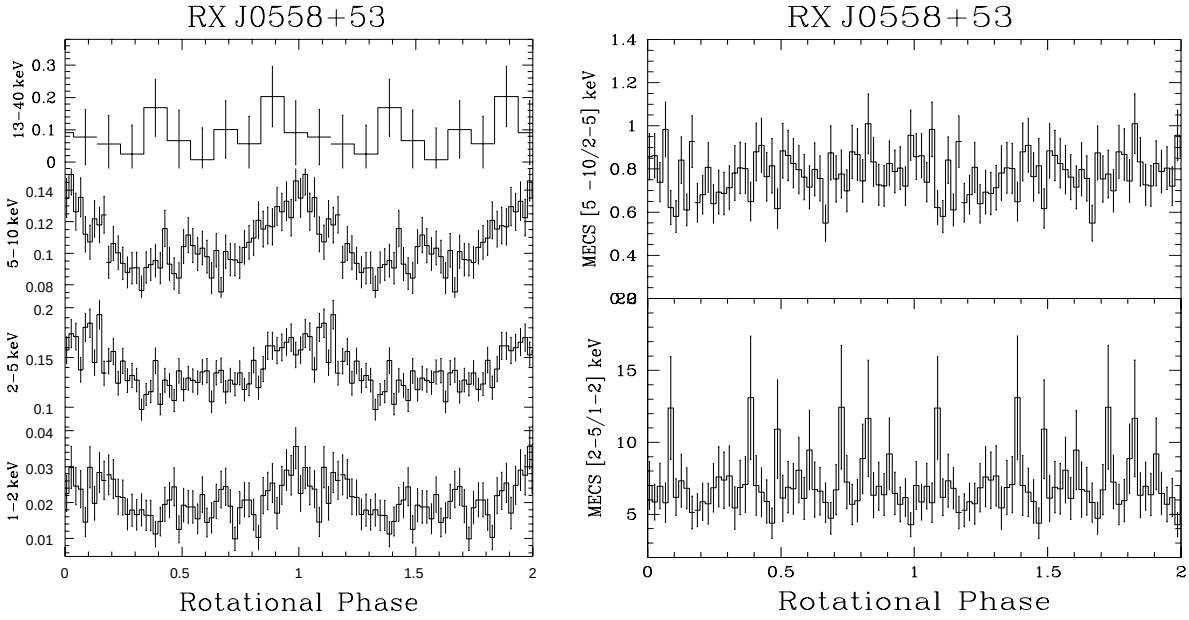

Fig. 2. Left: folded light curves for RX J0558 in different energy ranges from 1 to 40 keV using the ephemeris quoted in the text. **Right:** the hardness ratios in MECS bands show no spectral dependence of the spin pulsation (see text).

variations with spin phase, confirming the lack of energy-dependent modulation in the hard bands. The spin variability of the hard component is then due to aspect angle changes of the emitting region.

3.2. The spin modulation in RE 0751

RE 0751 was the first soft X-ray IP to be discovered from the ROSAT survey (Mason et al. 1992). A period derivative $\dot{P} = 1.1 \times 10^{-10}\,\mathrm{s\,s^{-1}}$ was subsequently found from X-ray and optical timings of the 833 s white dwarf rotational period spanning five years (Mason 1997), indicating that the white dwarf is spinning down at the largest rate ever found in an IP. Its behaviour in both soft and hard X-ray bands has never been monitored simultaneously. The BeppoSAX MECS (1–10 keV) light curve reported in Fig. 3 (left panel) clearly shows the presence of rapid pulses and the absence of variability at the 5.2 h orbital period. The DFT and CLEANED power spectrum in the LECS 0.1–0.4 keV, 0.4–1 keV and MECS 1–10 keV range are reported in the right panels of Fig. 3. Above 1 keV, the power spectrum shows a strong signal at the 833 s spin period and higher harmonics up to the third. In the 0.4–1 keV range, instead, the signal at these frequencies is at the noise level. Here the CLEAN algorithm does not detect even the base frequency. Below 0.4 keV the signal at the base frequency is strong again, but not those at the higher harmonics. This indicates that the 833 s modulation is structured in the hard X-rays, then mostly disappears at decreasing energies and appears again as a strong single pulse below 0.4 keV.

The energy dependent behaviour of the spin modulation has been inspected in different energy bands from 0.1 to 40 keV. In Fig. 4, we report the folded rotational pulses using the quadratic ephemeris provided by Mason (1997), which is based on the stable presence of a narrow dip and is accurate enough to extrapolate to the BeppoSAX observation epoch (i.e. the propagated phase error is $\delta\phi = 0.03$). The light curves confirm the very complex morphology, detected previously by ROSAT, Ginga, ASCA and RXTE (Duck et al. 1994; Mason 1997; Kiziloglu et al. 1998; James et al. 2002). In the 0.1–0.4 keV band (as well as in the 0.1–0.5 keV one, used by Duck et al. 1994) the pulse profile is single peaked, with count rates increasing by a factor of 4, with a hardly detectable narrow dip of 0.06 ± 0.01 width in phase. In the higher 0.4–1 keV range, the dip increases in breadth (0.1 in phase) and in place of the broad minimum observed in the softer band, a secondary maximum is observed, making the overall modulation highly structured, with large excursions throughout the spin cycle. The modulation at energies higher than 1 keV shows an increase in depth of the dip feature up to 5 keV. When compared to GINGA or ASCA data, the pulse is not double-peaked with primary and secondary maxima of the same intensity, but rather consists of a more structured primary maximum and a weaker secondary maximum which is detected up to 5 keV. Alternatively, a secondary dip at $\phi = 0.55$, more pronounced in the 2–5 keV range, might be present, simulating a double-peaked light curve. The modulation becomes very sinusoidal at 5–10 keV, with no apparent hint of a secondary maximum, which is instead observed by Ginga and broadly resembles that observed by RXTE (James et al. 2002). In the harder band (10–40 keV), again, we cannot detect any modulation due to the limited statistics of PDS data. The BeppoSAX data confirm the energy dependence of the dip which is not visible above 5 keV. The hardness ratios [5–10/2–5 keV] and [0.4–1/0.1–0.4 keV] show a different behaviour. Above 2 keV, the spectrum hardens during the dip and it is still hard at spin maximum and is softer at spin minimum. A hardening is also observed around phase 0.55. This confirms that the dip as well as the underlying modulation is energy dependent. There is probably an additional absorption component that produces the secondary dip, thus indicating that the absorbing material in the accretion flow is very structured. On

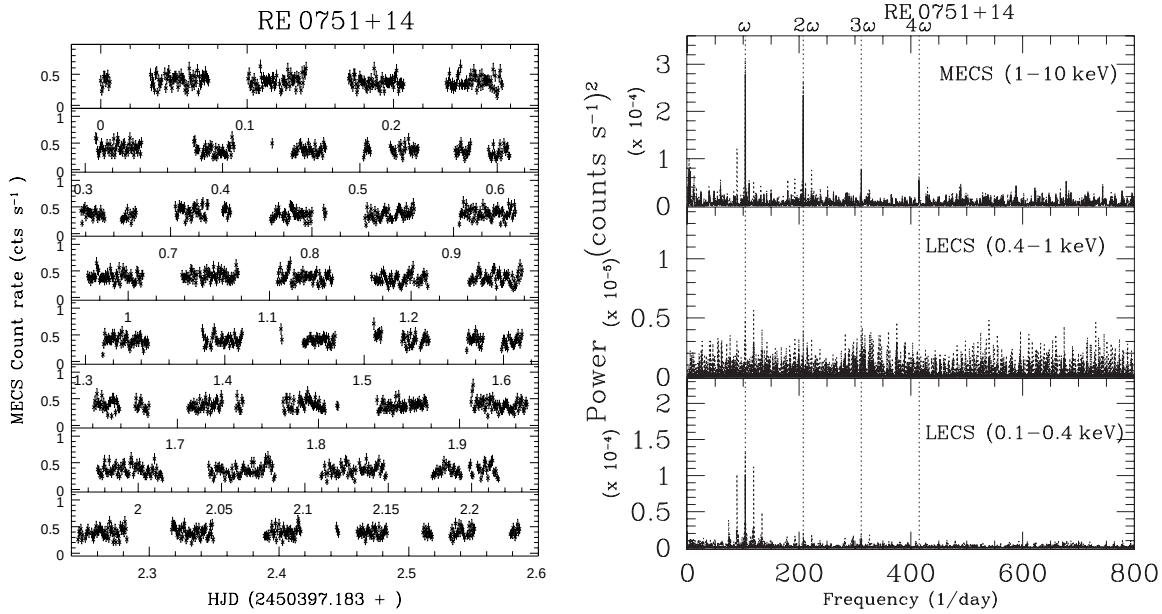

Fig. 3. Left: the net 60 s binned light curve of RE 0751. **Right:** the DFT (dotted line) and CLEANED (solid line) spectra in the MECS (1–10 keV), and two LECS (0.1–0.4 keV) and (0.4–1 keV) bands. The hard X-rays show strong signals at the 833 s frequency and higher harmonics. The softer band is instead dominated by the spin frequency only, while in the 0.4–1 keV band the spin signal is not significant.

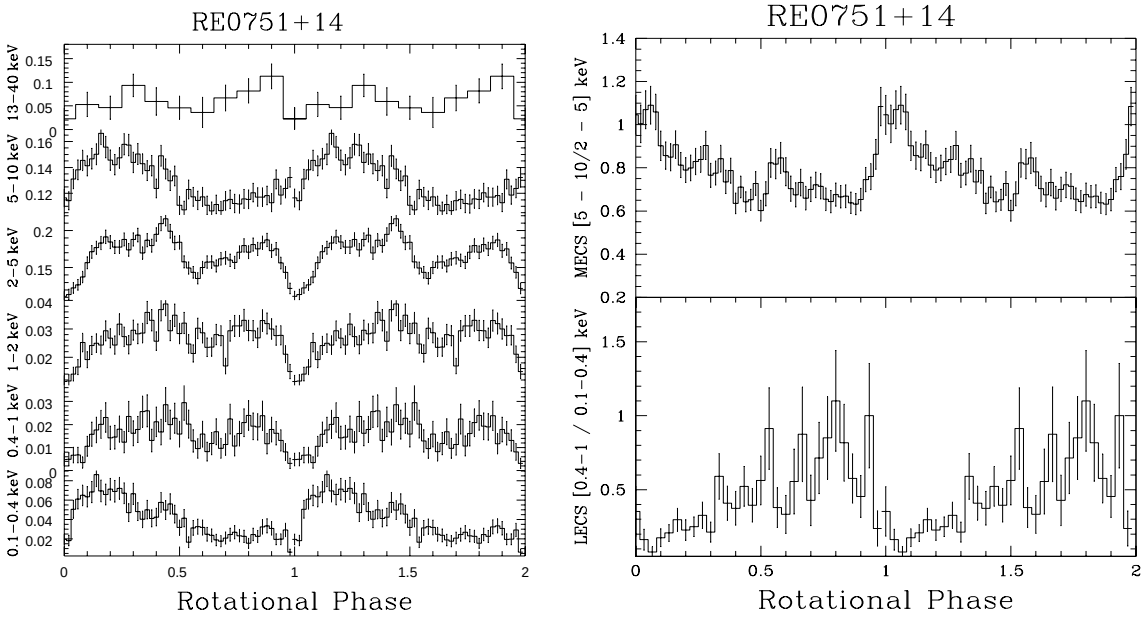

Fig. 4. Left: folded light curves of RE 0751 in different energy ranges from 0.1 to 40 keV using Mason's quadratic ephemeris (1997). **Right:** the hardness ratios in two soft LECS bands and two MECS bands show substantial differences.

the other hand, the soft X-rays harden at spin minimum, implying that either the X–ray reprocessing region is hardest, or that there is an additional contribution of a harder emitting region seen at spin phases between 0.6–0.9. This aspect will be reconsidered in Sects. 4 and 5.

3.3. The beat pulsation of RX J1712

This system was discovered as a hard X-ray IP (Haberl & Motch 1995) pulsating at a period of 1003 s, but with a 927 s period in its optical polarised light (Buckley et al. 1995, 1997). This led to the identification of the longer 1003 s period as the synodic period between the 3.42 h orbital and the 927 s white dwarf spin periods, thus making RX J1712 the only discless IP known so far, where accretion occurs via pole-flipping each half of a beat cycle. The MECS (1–10 keV) band light curve is shown in the left panel of Fig. 5. The DFT and CLEANED power spectra are reported in the right panels of that figure. A strong signal at the synodic frequency is detected in the harder bands (>1 keV), whilst in the softer 0.1–1keV range this frequency is not detected, although evidence of power is found between between 100 and 190 d^{-1}. No power is

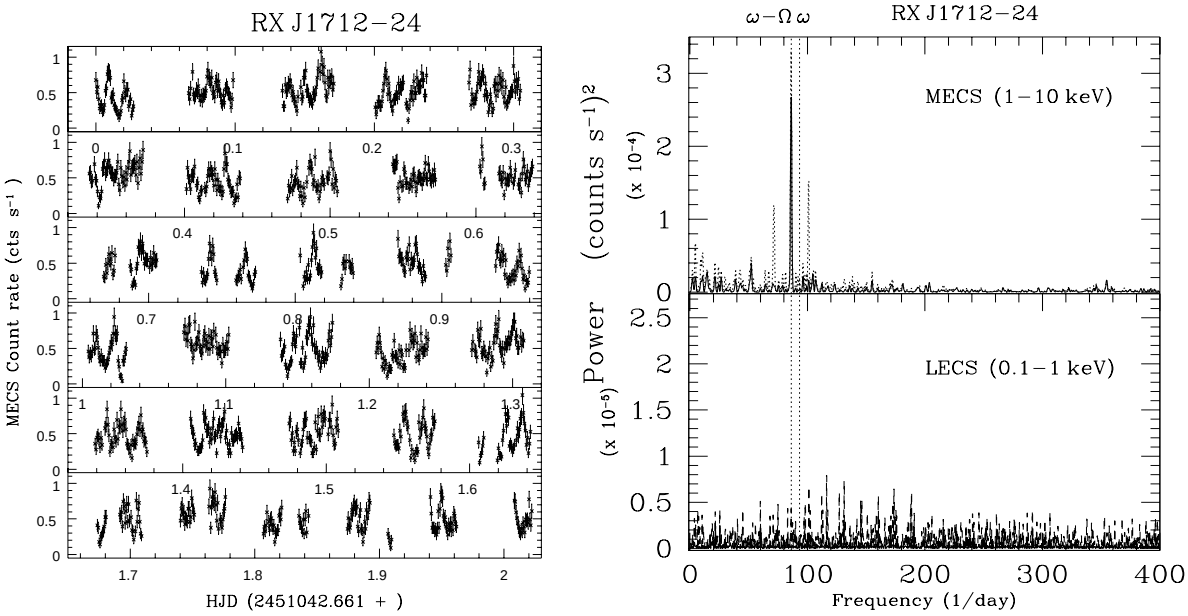

Fig. 5. Left: the net MECS 60 s binned light curve of RX J1712. **Right:** the DFT (dotted line) and CLEANED (solid line) spectra in the MECS (1–10 keV), and LECS (0.1–1 keV) bands. The hard X-rays are strongly modulated at the 1003 s synodic period while the soft X-ray band appears to be unmodulated at this frequency.

observed at the 927 s spin and 3.42 h orbital frequencies, confirming the ROSAT and RXTE results (Hellier & Beardmore 2002). Consistency checks on the LECS data have been carried out and the strong beat pulsation is present in different bands above 1 keV.

To study the energy dependence of beat pulses, we obtained the time of X-ray maximum for our BeppoSAX data set by a sinusoidal fit to the MECS (1–10 keV) light curve: $\mathrm{HJD_{max}}$ = 2 451 063.62405(5). We then folded the light curves in different energy bands as shown in Fig. 6 (left panel). The modulation is stronger in the hard bands, with a pulsed fraction of 80% in the 5–10 keV range, 60% in the 2–5 keV band and 50% in the 1–2 keV range. In this latter range the modulation is not sinusoidal, with a structured minimum. The 0.1–1 keV range instead shows excursions up to 60% over the synodic cycle, although an underlying sinusoidal trend might be present. The softer bands (below 2 keV) might be indicative of a different emission component. A hardening at pulse maximum is observed above 2 keV, while at lower energies no variations are detected (Fig. 6, right panels). The hardening at pulse maximum in this discless system is similar to that observed in Polars (Matt et al. 2000), which accrete via a column fed directly from the stream. Hence, pulse maxima are observed when the column points towards the observer and the absorption is maximum, with the hardest regions contributing most. The lack of strong pulsations below 1 keV and the fact that the X-ray modulation does not vanish at pulse minimum (which is seen in Polars) suggest an additional source of X-rays. This aspect will be discussed in Sect. 5.

4. The broad-band spectral properties

We studied the broad-band spectra by means of spectral fits (using XSPEC) to the phase–averaged spectra. We used the combined LECS, MECS and PDS data for RX J0558 and RE 0751 allowing the study from 0.1 to 90 keV. For RX J1712 we used the LECS and MECS data only and hence spectra are limited from 0.1 to 10 keV. We have adopted a composite model consisting of an isothermal plasma emission (MEKAL) with temperature kT_{hard} and metal abundance A (in number with respect to solar), a black–body component with temperature kT_{BB}, two cold media consisting of a simple absorber with column density N_{H} and a partial covering absorber with column density $N_{\mathrm{H(pcfabs)}}$ and covering fraction C_{F}. The model also includes a Gaussian fixed at $E = 6.4$ keV to account for the iron K_{α} fluorescent line and a Compton reflection component, with relative normalization R, which represents the solid angle subtended by the material in units of $2\,\pi$ for an average viewing angle fixed to 60°. The iron and other element abundances of this component (REFLECT in XSPEC) have been linked to the abundance of the MEKAL model. A Compton reflection component has been demonstrated to be present in mCVs (both Polars and IPs) (Done et al. 1995; Matt 1999; Ezuka & Ishida 1999; Matt et al. 2000; de Martino et al. 2001). Here we note that the BeppoSAX data are not of enough quality to derive the multi–temperature structure of the post–shock region. Indeed a power law temperature profile (CEMEKL in XSPEC) gives worse fits with respect to an isothermal plasma. Hence, we are unable to estimate the white dwarf masses as we lack reliable shock temperatures. In Table 2, we report the results of the spectral fits with the mentioned model, which are shown in Fig. 7. Here we note that for RX J1712, because of the lack of PDS data, we first assumed no reflection (i.e. $R = 0$). We also allowed for this parameter to change and obtained an upper limit of 0.16. This is however unrealistic for the large EW of the iron line and the low abundances and, therefore, we assumed $R = 1$.

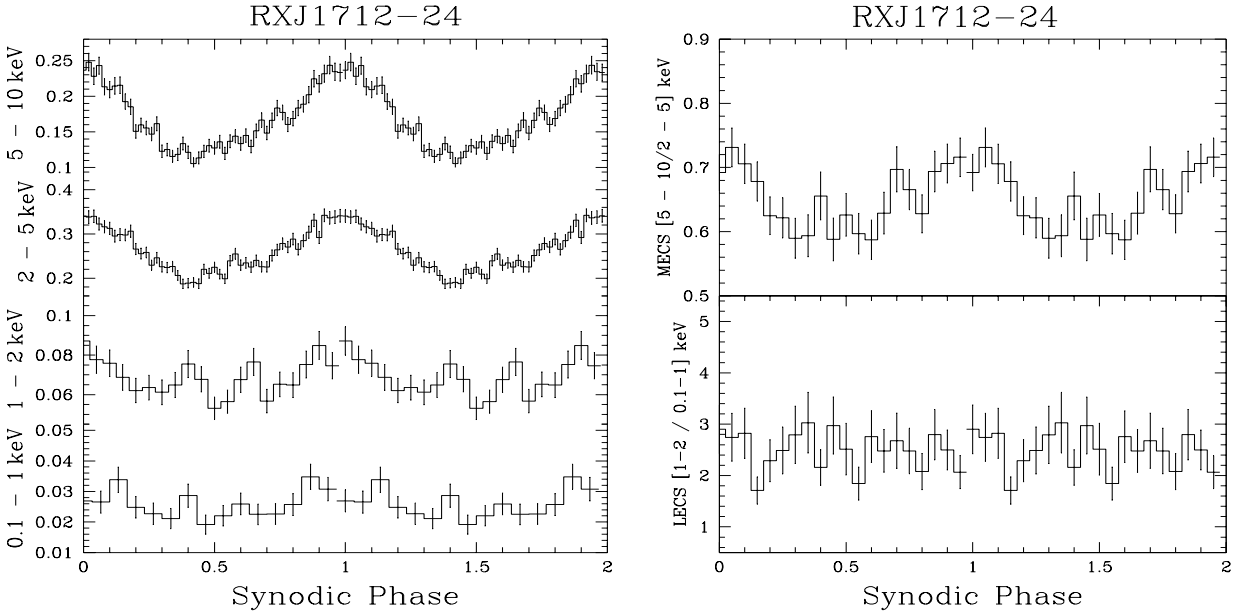

Fig. 6. Left: folded light curves of RX J1712 in different energy ranges from 0.1 to 10 keV. **Right:** the hardness ratios in two soft LECS bands and two MECS hard bands showing different behaviour with respect to other IPs.

Table 2. Spectral fits to the grand–average spectra of RE 0751, RX J0558 and RX J1712. The adopted model is described in the text. Quoted errors refer to 90% confidence level for the parameter of interest.

Parameter	RE 0751+14	RX J0558+53	RX J1712-24
$N_{\rm H}^1$	$0.58^{+1.27}_{-0.56}$	$3.7^{+2.6}_{-2.1}$	46^{+12}_{-13}
$N_{\rm H(pcfabs)}^2$	$4.8^{+2.8}_{-1.7}$	$5.1^{+2.7}_{-2.3}$	$11.8^{+4.1}_{-3.3}$
$C_{\rm F}$	$0.39^{+0.09}_{-0.08}$	$0.42^{+0.05}_{-0.04}$	$0.34^{+0.05}_{-0.06}$
$kT_{\rm BB}^3$	56^{+12}_{-14}	73^{+14}_{-14}	103^{+11}_{-9}
$kT_{\rm hard}^4$	17^{+2}_{-2}	34^{+21}_{-11}	13^{+1}_{-2}
$L_{\rm BB}/L_{\rm hard}$	∼0.4	∼0.8	∼0.7
A	$0.33^{+0.07}_{-0.09}$	$1.17^{+0.93}_{-0.55}$	$0.36^{+0.12}_{-0.10}$
EW^5	188±56	260^{+72}_{-80}	157^{+37}_{-34}
R^6	$2.2^{+1.1}_{-1.1}$	$1.2^{+1.7}_{-1.0}$	1.
$\chi^2_{\rm red}$	1.07	1.22	1.01

[1] Hydrogen column density accounting for the interstellar absorption in units of 10^{20} cm^{-2}.
[2] Column density of the partial absorber in units of 10^{22} cm^{-2}.
[3] Temperature in units of eV.
[4] Temperature in units of keV.
[5] Equivalent width of the 6.4 keV Gaussian in units of eV.
[6] Relative normalization of the reflection component in units of 2π. It is fixed in RX J1712 (see text).

For all three sources, the column densities of the simple absorber are compatible within errors with the ROSAT determinations (Haberl & Motch 1995; Duck et al. 1994) and are also in agreement with the estimates of E_{B-V} obtained from UV spectra (Mouchet et al. 1998; de Martino et al. 1998). These are lower or at most equal to the galactic column densities in the direction of the three sources, implying that the simple absorber can be regarded as of interstellar origin. From the fits, the partial covering (up to 40%) cold absorber has instead much higher densities than that of the galactic medium and its origin is intrisic to the systems. As will be seen in Sect. 4.1, this intrinsic absorber is likely to be more complex, but this approximation allows us to identify in a simple way, the presence of localized cold material close to the X-ray source.

The black–body component is found to be ubiquitous in all three systems with temperature that are at the higher end of the temperature range found in Polars (20–60 eV). The hottest black–body component is found in RX J1712 (100 eV) which confirms the surprising results of Haberl (2002) obtained from XMM–Newton observations for this source and 1RXS J154814.5-452845 (Haberl et al. 2002). Very hot temperatures are not observed in Polars. The relatively high black–body temperature in RX J0558 is within errors compatible with the earlier ROSAT results by Haberl & Motch (1995). For RE 0751, our spectral fit gives a slightly higher temperature but is still consistent within errors with that derived by Duck et al. (1994) from ROSAT observations at 46 eV, but not with the one determined from ASCA (James et al. 2002) which however was not well constrained. Here we note that James et al. (2002) also fix the temperature of this component to the ROSAT value in their ASCA phase–average spectral fit, but in the phase–resolved analysis the temperature is fixed to the value of 83 eV, found for the spectrum at maximum. The normalizations of the black–body components are loosely constrained (60–70% uncertainty).

The average temperature of the optically thin post–shock plasma is well constrained except for RX J0558 which also has a poorly determined abundance. For this parameter we also find indication of underabundances in RX J1712 and RE 0751. Ezuka & Ishida (1999) also find that magnetic CVs generally display subsolar iron abundances. The temperatures of the hard X-ray component are substantially lower than those derived excluding the reflection, which is however required by the data.

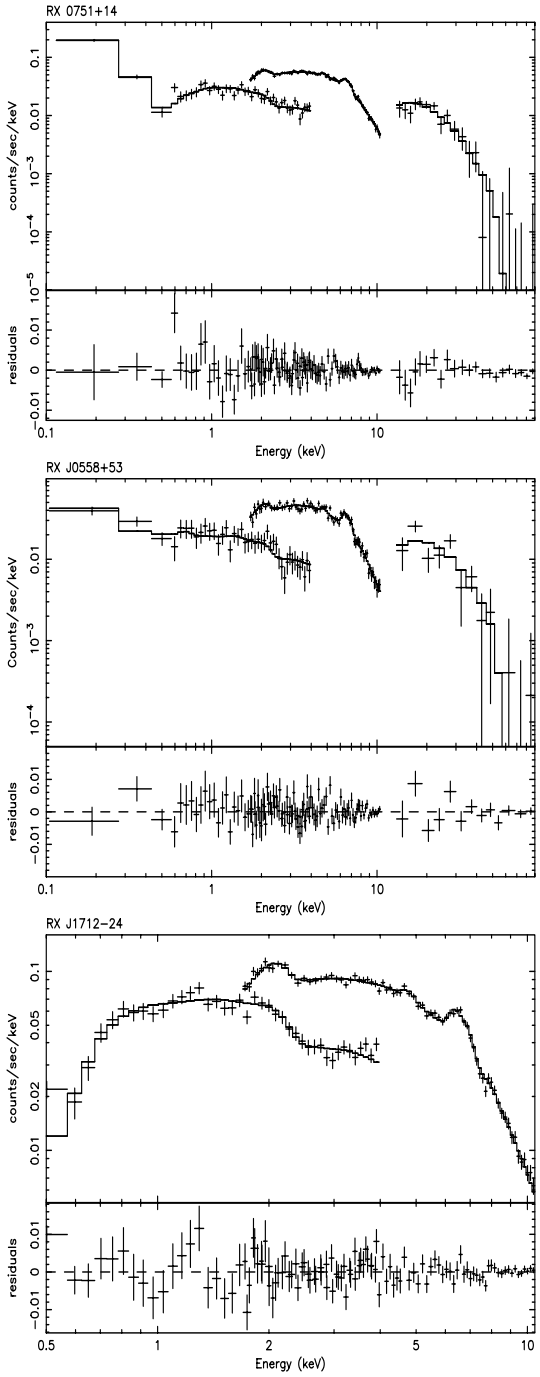

Fig. 7. From top to bottom: the phase–averaged spectra of RE 0751, RX J0558 and RX J1712 along their best fit model described in Table 2. Lower panels show the residuals.

The 6.4 keV iron line *EW*s are too large to be accounted for by the partial covering absorber (Inoue 1985; Matt 2002), and they are likely produced by the white dwarf surface along with the Compton reflection component (Matt 1999), as also found for the IP RX J0028.8+5917 (de Martino et al. 2001). For RE 0751, the line *EW* is consistent with the measured value of *R*, even allowing for the low iron abundance (Matt et al. 1997). The same is true for RX J0558 when the rather large errors are considered, even if the value of *EW*, taken at face value, appears rather large when compared to *R*. For RX J1712, the value of *R* is very loosely constrained due to the lack of usable PDS data; for this source, a non-negligible contribution from the partial covering absorber is also expected, given the large column density. Although poorly constrained, the ratios between bolometric black–body and hard X-ray components are found to be close to unity in RX J0558 and RX J1712, and lower in RE 0751.

4.1. Phase–resolved spectral variations

To investigate in more detail the spectral behaviour of pulsations, we performed fits to the spectra at maximum and minimum of the pulse cycle of the three sources and also to the dip spectrum of RE 0751. We used only LECS and MECS data due to the lack of variability in the PDS. The spectral fits consist of a composite model of a MEKAL plus black–body component, the interstellar column density, the partial absorber and a Gaussian line fixed at 6.4 keV. For RE 0751 and RX J0558, we also included the reflection component as this is expected to be angle–dependent (Matt 1999). We have therefore fixed the interstellar hydrogen column densities to the values found from the fits of the phase–averaged spectra. Also the temperature and abundance of the optically thin plasma are fixed at the values obtained from the phase–averaged spectra. This was done because the former is an average temperature over the emitting post–shock region and the latter is not expected to change with phase. The temperature of the black–body, the partial covering parameters, the normalization of the Gaussian and those of the hard and black–body components as well as the reflection parameter are kept free. In Table 2 we report the results of the spectral fits for the three systems.

RX J1712 shows an increase of the partial covering absorber (both in column density and covering fraction) at beat maximum which is consistent with the behaviour observed in the hardness ratios (hardening at maximum). On the other hand, the fits do not indicate variations of the temperature of the black–body component. The normalizations of the black–body and of the optically thin component increase at beat maximum and thus the ratio of their bolometric luminosities remains constant. This implies that the spectral changes are due to variations of the absorber and of the normalizations of the black–body and of the hard X-ray component. The *EW* of the 6.4 keV iron line obtained for these two phases does not vary within errors. The unabsorbed bolometric flux of the hot black–body component ranges between $1.1–0.64\times10^{-10}$ erg cm^{-2} s^{-1} at beat maximum and minimum respectively. The lack of clear modulation at the synodic frequency in the softest band might then be due to the concurrence of phasing of the high density absorbing material which increases when the black–body area is largest.

RX J0558 shows a different behaviour; the partial covering absorber (both column density and covering fraction) is constant within errors at spin maximum and minimum. The spin variability is then only due to changes in the normalization of the optically thin component which varies by a factor of 1.3 between the two phases. The black–body component is constant due to the lack of variability in the LECS data. Its average unabsorbed bolometric flux is $\sim4\times10^{-11}$ erg cm^{-2} s^{-1}. The ratio

between this and that of the optically thin component slightly increases at spin minimum, due to the decrease in the normalization of the hard X-ray emission at this phase. The *EW* of the iron K_α line does not change within the errors, although taking the *EW* and *R* at their face values at spin minimum, a decrease might be suggested. The lack of spectral changes does not allow us to isolate the secondary pole in the hard X-rays at the minimum of the spin pulse.

In RE 0751, we infer a different spectral behaviour with respect to the other two sources. The temperature of the black–body component as well as the *EW* of the iron fluorescent line and reflection do not change with spin phase. The normalization of the black–body component is about the same during the maximum and the dip and larger than that during minimum by a factor of about 3. The unabsorbed bolometric black–body flux at maximum and dip is $\sim 3\times10^{-11}$ erg cm^{-2} s^{-1}. This indicates that the overall soft spin modulation is essentially due to changes in the projected area of the black–body, with no indication of an additional component. The partial absorber largely covers the X-ray source during the dip but with a lower column density, suggesting photo-electric absorption by an intervening phase–dependent and very localized material. The reflection is unrealistically high during the dip, but it indicates that the cold material is facing the observer. The partial covering absorber is also larger (both column density and covering fraction) at spin maximum. The emission measure of the optically thin component $EM = 2.5 \pm 0.4 \times 10^{55}$ cm^{-3}, linked to its normalization, changes by a factor of 1.2 between maximum and minimum, but during the dip it is lower by a factor of 2. Why the emission measure of the hard X-ray component is lower during the dip phases is not understood. The ratio of the bolometric fluxes of the black–body and the optically thin component is about unity during the dip and it is much lower during maximum and minimum (0.5 and 0.2 respectively). Then, the overall pulsation at higher energies is due to absorbing material which is different from that causing the dip. The different shapes of the modulation between 0.4 and 5 keV are likely due to an even more complex and structured absorbing material, for which our simple modeling of the spectra at the three spin phases cannot account. Indeed Duck et al. (1994), and similarly Kiziloglu et al. (1998), use in their spectral fits two columns with different densities (10^{22} and 10^{23} cm^{-2}), but the latter is not constrained from their data. However, and unlike Duck et al. (1994), who conclude that the general rotational modulation is only due to the normalization of each spectral component, we find that it is true only for the black–body.

5. Discussion

In these systems, the pulsations are complex and different from each other. The basic difference is that RX J0558 and RE 0751 are disc–fed systems, while RX J1712 is a disc–less accretor. All of them are characterized by a soft and relatively hot (60–100 eV) and a hard (13–30 keV) optically thin component whose behaviour at the dominant periodicity reveals great differences.

RX J0558 was known to show a single-peaked pulsation at the spin period of the white dwarf in the hard X-rays, but a double–peaked pulse in the soft bands. We cannot derive constraints on the soft X-ray variability due to limitations of the LECS data. The lack of spin variation of the partial absorbing material does not fit with the general picture of IPs, where spin pulses are due to aspect angle changes of the emitting regions combined with photoelectric absorption in the accretion curtain fed by the disc. Allan et al. (1996) and Norton et al. (1999) proposed that rapid rotators, like RX J0558, possess weak magnetic fields, allowing the accretion material to flow onto large surface areas of the white dwarf. In this configuration the optical depth along the curtain is smaller than perpendicularly and, hence, absorption effects, as seen by the observer, can be opposite to those encountered in high field IPs. This modified accretion scenario is not supported by either our observations or ROSAT data (Haberl et al. 1994), where the 0.1–2.4 keV pulses did not show any energy dependence. Also, optical polarized radiation has been detected in RX J0558 (Shakhovskoj & Kolesnikov 1997), indicating that the magnetic field can be as high as that in RE 0751 and RX J1712. Furthermore, since RX J0558 shows a double humped soft X-ray light curve in other observations, both poles are visible and hence its inclination is likely larger than 40°. The lack of X-ray eclipses also gives an upper limit of 80° to the binary inclination. In this range, we should expect changes in the absorption with the spin phase, unless the absorbing material is far away from the X-ray emitting region. For this system the black–body and optically thin component mostly balance and hence, we use the hard X-ray luminosity to estimate the accretion rate. Assuming a white dwarf mass in the range 0.6–1.1 $M_\odot$ (the latter from Ramsay 2000), we derive $\dot{M} \sim 3\text{–}5 \times 10^{14}\,(d/100\,\mathrm{pc})^2$ g s^{-1}. Due to the lack of magnetic field measures and knowledge of the distance, we cannot derive the Alfven radius to infer up to what distance the absorbing material might be located.

In RE 0751, the spin modulation is highly structured and energy dependent, confirming previous results (Duck et al. 1994). We find that details of the medium energy pulsation change with respect to previous observations and we derive simultaneous information on the soft and hard spectral components. The energy-dependent pulses are affected by absorption from material partially covering the X-ray source, but with a phase behaviour (minimum at spin minimum), which is not expected from the classical accretion curtain scenario. The dip feature is due to further intervening phase–dependent material in the accretion flow which mostly (70%) covers the X-ray source. The soft X-ray pulsation is instead due to variations in the projected area of the X–ray irradiated polar region. A strong magnetic field (9–21 MG) has been estimated, with a dipole offset of 30^o and an inclination angle of 60^o, allowing two extended arc-shaped accreting regions, placed ahead of the magnetic poles (Potter et al. 1997). In this model, material couples at large radii and travels out of the orbital plane, producing large absorption effects when the accretion region passes through the line of sight at some phases and in particular the dip. At pulse maximum and at the dip, the projected area of the black–body component and the absorption are largest, in agreement with Potter et al.'s model. The ratio of the bolometric black–body and the hard X-ray luminosities is quite low and different from that derived by Duck et al. (1994) who instead

Table 3. Spectral fits to the maximum and minimum spectra of RE 0751, RX J0558 and RX J1712. For RE 0751 the dip spectrum fit is also reported.

Parameter	RE 0751+14			RX J0558+53		RX J1712-24	
	Maximum	Minimum	Dip	Maximum	Minimum	Maximum	Minimum
$N^1_{\rm H(pcfabs)}$	$9.0^{+3.3}_{-1.4}$	$8.3^{+4.8}_{-3.8}$	$1.0^{+0.3}_{-0.2}$	$8.3^{+5.1}_{-4.9}$	$6.1^{+2.9}_{-2.0}$	$16.3^{+4.5}_{-3.6}$	$9.6^{+4.3}_{-3.4}$
$C^2_{\rm F}$	$0.51^{+0.06}_{-0.08}$	$0.36^{+0.09}_{-0.12}$	$0.72^{+0.04}_{-0.03}$	$0.40^{+0.06}_{-0.11}$	$0.48^{-0.06}_{+0.08}$	$0.41^{+0.03}_{-0.02}$	$0.26^{+0.03}_{-0.02}$
$kT^3_{\rm BB}$	58^{+5}_{-6}	56^{+14}_{-12}	53^{+7}_{-6}	77^{-11}_{+10}	77^{+8}_{-7}	105^{+16}_{-13}	108^{+17}_{-14}
$L_{\rm BB}/L_{\rm hard}$	∼0.5	∼0.2	∼1	∼0.4	0.6	∼0.6	∼0.6
EW^4	175^{+57}_{-54}	165^{+62}_{-61}	196^{+142}_{-158}	290^{+66}_{-80}	260±90	152^{+50}_{-51}	174^{+56}_{-29}
R^5	$0.7^{+0.96}_{-0.7}$	< 0.7	$7.7^{+0.1}_{-1.5}$	< 2	< 0.7	1.	1.
$\chi^2_{\rm red}$	0.98	1.20	0.96	1.01	1.23	1.11	0.96

[1] Column density of the partial absorber in units of 10^{22} cm^{-2}.
[2] Covering fraction of partial absorber.
[3] Temperature in units of eV.
[4] Equivalent width of the 6.4 keV Gaussian in units of eV.
[5] Relative normalization of the reflection component in units of 2π.

found 2.2–1.5, compared to our 0.5. We note that RE 0751 was at a similar flux level as that observed during ROSAT observations. The differences are, however, within the errors of our bolometric fluxes. Given the lack of balance between these fluxes in our fits, we use again the bolometric luminosity of the hard X-ray component to estimate the mass accretion rate. Adopting a distance of 400 pc (Patterson 1994), we derive a luminosity of $8.3{\times}10^{32}$ erg s^{-1}, and, assuming a white dwarf mass between 0.6–1.35 $M_\odot$ (the latter from Cropper et al. 1998), we derive $\dot{M} = 2$–$8{\times}10^{15}$ g s^{-1}. Adopting a value for the magnetic moment of $3{\times}10^{33}$ G cm^3, obtained for a 15 MG field and an average radius corresponding to the above mass range, and using the derived mass accretion rate, we find that the Alfven radius $r_{\rm A} = 0.52(\mu_{\rm WD})^{4/7}\,(2{\rm GM_{WD}})^{-1/7}\,(\dot{M})^{-2/7} \sim 4\times10^{10}$ cm. This implies that indeed the material can be captured at large radii.

In RX J1712, the pulsation at the synodic period indicates a disc–less accretion, which switches from one pole to the other each half of a beat cycle. Hence, differently from Polars or disc–fed IPs, where the spin modulation is purely geometrical, in stream–fed systems the poles experience changes in mass accretion rate. As already pointed out by Buckley et al. (1997) and Hellier & Beardmore (2002), the pulsation is not total, implying that an accreting region is visible during the inter–pulse phases. The absence of an orbital variability typically expected in a disc–less configuration indicates that RX J1712 is a low inclination system. Indeed, a 10^o inclination is reported by Buckley et al. (1995) and hence the secondary pole is never observed and the primary pole is mostly visible throughout the spin cycle. Our data do not support an additional emitting region in both soft and hard X-rays. It is thus possible that the pole flipping is not total, with the primary pole still accreting but at a lower level, so that at beat minimum we are still viewing parts of the accretion flow. Then, when the visible pole is accreting at a higher rate (beat maximum), a higher flux and higher absorption are expected as is observed. To account for the low amplitude of the beat modulation, Hellier & Beardmore (2002) suggest that the accretion involved in the pole–flipping is only 25 percent of the total flow. The remaining material is circulating in a diamagnetic blob flow threading the magnetosphere and forming a non–coherent accretion curtain, thus making the spin pulsation undetectable. If so, it is reasonable to expect spectral changes during the faint phase but our spectral fits do not show this in both soft and hard X-ray components. Since the bolometric luminosities of the black–body and optically thin components roughly balance, we use the hard X-ray bolometric luminosity to estimate the accretion rate. We assume a conservative distance of 50 pc (Väth 1997) and a 0.7 $M_\odot$ white dwarf (Ramsay 2000), thus giving $\dot{M} \sim 3\times10^{14}$ g s^{-1}, which changes by a factor of ∼1.7 between maximum and minimum of the beat pulse.

6. Conclusions

We have presented the first simultaneous soft and hard X-ray data of the three soft X-ray IPs, RE J0751, RX J0558 and RX J1712, over the wide energy range of the BeppoSAX satellite. All three sources have strong X-ray modulation at periods identified as the white dwarf rotations in RX J0558 and RE 0751, and as the synodic period in RX J1712. We have inferred the temperatures of both post–shock flow and of the irradiated polar region of the white dwarf. The temperatures of the black–body component are very high, up to 80–100 eV in RX J0558 and RX J1712, much higher than those found in the Polars. The temperature of the hard X-ray emitting region is found between 13–30 keV. Furthermore, a Compton reflection component is definitely present in RX J0558 and RE 0751, while in RX J1712 it is favoured. The reflection likely originates at the white dwarf surface.

In the three systems, we find differences in the periodic behaviour of the spectral components. We find that the absorbing material partially covering the X-ray source is

phase–dependent in RE 0751 and RX J1712 but not in RX J0558. The column densities can be as high as 10^{23} cm^{-2}, as in RX J1712, which can heavily hamper the detection of soft X-rays in other hard X-ray IPs.

Although these soft X-ray IPs share common properties, their X-ray temporal and spectral characteristics suggest accretion patterns that cannot be reconciled with a single and simple configuration.

Acknowledgements. DdM and GM acknowledge financial support from ASI.

References

Allan, A., Horne, K., Hellier, C., et al. 1996, MNRAS, 279, 1345
Beardmore, A. P., Done, C., Osborne, J. P., et al. 1995, MNRAS, 272, 749
Boella, G., Butler, R. C., Perola, G. C., et al. 1997, A&AS, 122, 299
Buckley, D. A. H., Sekiguchi, K., Motch, C., et al. 1995, MNRAS, 275, 1028
Buckley, D. A. H., Haberl, F., Motch, C., et al. 1997, MNRAS, 287, 117
Burwitz, V., & Reinsch, K. 2001, ed. N. White, G. Malaguti, & G. C. Palumbo, AIP Conf. Ser., 599, X-ray Astronomy: Stellar Endpoints, AGN and Diffuse Background, 522
Cropper, M., Ramsay, G., & Wu, K. 1998, MNRAS, 293, 222
Deeming, T. J. 1975, Ap&SS, 36, 137
de Martino, D., Mouchet, M., & Bonnet-Bidaud, J.-M. 1998, ESA SP-413, 427
de Martino, D., Matt, G., Mukai, K., et al. 2001, A&A, 377, 499
Done, C., Osborne, J. P., Beardmore, A. P. 1995, MNRAS, 276, 483
Duck, S. R., Rosen, S. R., Ponman, T. J., et al. 1994, MNRAS, 271, 372
Ezuka, H., & Ishida, M. 1999, ApJS, 120, 277
Haberl, F. 2002, ed. B. T. Gäensicke, K. Beuermann, & K. Reinsch, ASP Conf. Ser., 261, The Physics of Cataclysmic Variables and Related Objects, 151
Haberl, F., Motch, C., & Zickgraf, F.-J. 2002, A&A, 387, 201
Haberl, F., Thorstensen, J. R., Motch, C., et al. 1994, A&A, 291, 171
Haberl, F., & Motch, C. 1995, A&A, 297, L37
Hellier, C. 1991, MNRAS, 251, 693
Hellier, C., & Beardmonre, A. P. 2002, MNRAS, 331, 407
Ishida, M., Mukai, K., & Osborne, J. P. 1994, PASJ, 46, L81
Kizilogly, Ü., Baykal, A., Alev, M., et al. 1998, Ap&SS, 259, 191
James, C. H., Ramsay, G., Cropper, M., et al. 2002, MNRAS, 336, 550
Mason, K., Watson, M. G., Ponman, T. J., et al. 1992, MNRAS, 258, 749
Mason, K. 1997, MNRAS, 285, 493
Matt, G., Fabian, & Reynolds, C. S. 1997, MNRAS, 289, 175
Matt, G. 1999, Annapolis Workshop on Magnetic Cataclysmic Variables, ed. C. Hellier, & K. Mukai, ASP Conf. Ser., 157, 299
Matt, G., de Martino, D., Gäensicke, B. T., et al. 2000, A&A, 358, 177
Matt, G. 2002, MNRAS, 337, 147
Mouchet, M., Bonne-Bidaud, J.-M., & de Martino, D. 1998, ESA SP–413, 431
Mukai, K., Fujimoto, R., & Hellier, C., et al. 1997, communication poster at the ASCA Cherry Blossom Workshop, Washington, DC
Norton, A. J., Watson, M. G., King, A. R., et al. 1992, MNRAS, 254 705
Norton, A. J., Beardmore, A. P., Allan, A., et al. 1999, A&A, 347, 203
Potter, S. R., Cropper, M., Mason, K. O., et al. 1997, MNRAS, 285, 82
Patterson, J. 1994, PASP, 106, 209
Ramsay, G. 2000, MNRAS, 314, 403
Roberts, D. H., Lehár, J., & Dreher, J. W. 1987, AJ, 93, 968
Rosen, S. R., Mason, K. O., & Cordova, F. A. 1988, MNRAS, 231, 549
Shakhovskoj, N. M., & Kolesnikov, S. V. 1997, IAUC, 6760
Skillman, D. 1996, PASP, 108, 130
Väth, H. 1997, A&A, 476, 486
Wynn, G., & King A. 1992, MNRAS, 255, 83